Stability of ferroelectric and antiferroelectric hafnium–zirconium oxide thin films

Kisung Chae, Jeongwoon Hwang, Evgueni Chagarov, et al.

View Online   Export Citation   CrossMark

ARTICLES YOU MAY BE INTERESTED IN

Stability of ferroelectric and antiferroelectric hafnium–zirconium oxide thin films

Kisung Chae,[1,2] (ID) Jeongwoon Hwang,[2,3] Evgueni Chagarov,[1] Andrew Kummel,[1,a] and Kyeongjae Cho[2,a] (ID)

AFFILIATIONS

[1]Department of Chemistry and Biochemistry, University of California San Diego, 9500 Gilman Dr, La Jolla, California 92093, USA
[2]Department of Materials Science and Engineering, The University of Texas at Dallas, 800 W Campbell Rd, Richardson, Texas 75080, USA
[3]Department of Physics Education, Chonnam National University, 77 Yongbong-ro, Yongbong-dong, Buk-gu, Gwangju 61186, South Korea

[a])**Authors to whom correspondence should be addressed:** akummel@ucsd.edu and kjcho@utdallas.edu

ABSTRACT

Hafnium–zirconium oxide (HZO) thin films are of interest due to their ability to form ferroelectric (FE) and antiferroelectric (AFE) oxide phases. Density functional theory is employed to elucidate the stabilization mechanisms of both FE HZO thin films and AFE ZrO_2 films. The FE orthorhombic phase is primarily stabilized by in-plane tensile strain, which spontaneously occurs during the synthesis process, and this is more effective for HZO than HfO_2. Layer-by-layer stack models and core-matrix three-dimensional models of the polymorphs reveal that the electrostatic component of interfacial free energy can play a critical role in the formation of the AFE tetragonal phase in ZrO_2 and the "wake-up" effect for FE HZO.

I. INTRODUCTION

The demonstration of ferroelectricity in hafnium oxide (HfO_2)-based thin films such as $Hf_{0.5}Zr_{0.5}O_2$ (HZO) and doped HfO_2[1,2] has triggered intense research efforts because they may be a key component for next-generation electronic devices such as negative capacitance field effect transistors[3] and ferroelectric (FE) memories.[4] HZO films show large bandgaps, high dielectric constants, and robust ferroelectric behavior in films with a thickness of ∼10 nm.[1,2] HZO is considered especially promising compared to doped HfO_2 since there is a broad process window that induces FE behavior in HZO thin films.[5]

It is generally accepted that the orthorhombic $Pca2_1$ phase is responsible for the observed ferroelectricity in HZO thin films.[1,2] It is a metastable phase in bulk crystals since the formation energy is ∼70 meV per formula unit (fu) higher than the ground state monoclinic $P2_1/c$ phase according to density functional theory (DFT) calculations [see Fig. 1(b)]. A number of factors have been suggested to stabilize the ferroelectricity in HZO thin films such as the thickness and composition of the film as well as the top/bottom electrode materials.[1,2,6–8] Thinner films with a composition close to

50% Hf and 50% Zr tend to favor ferroelectricity.[6] In addition, ferroelectricity is favored for HZO films grown on specific electrode materials. Titanium nitride (TiN)[6,7] and tungsten (W)[9] are well-known to favor the ferroelectricity in HZO while Pt electrodes cannot form ferroelectric HZO films.[10] In contrast to the inert Pt electrodes, both TiN and W electrodes are known to form strong interfacial bonding with HZO, which is a key factor for inducing ferroelectricity in HZO.

While some of these factors are recognized as important by various research groups, most of the theoretical predictions based on DFT calculations argue that compressive strain is responsible for the stabilization of the FE orthorhombic phase over the monoclinic phase.[11,12] However, experimental studies often report that the ferroelectric HZO {111} films exhibit tensile stress.[13] For instance, Batra *et al.* show in their DFT calculations that compressive strain with an external electric field can stabilize the orthorhombic phase with both hydrostatic and in-plane (001) stress conditions.[11] Similarly, Liu and Hanrahan also show the effects of in-plane strain for {100}, {110}, and {111} HZO, arguing that ferroelectricity can be stabilized either by in-plane compression for those orientations or by an external electric field.[12] These
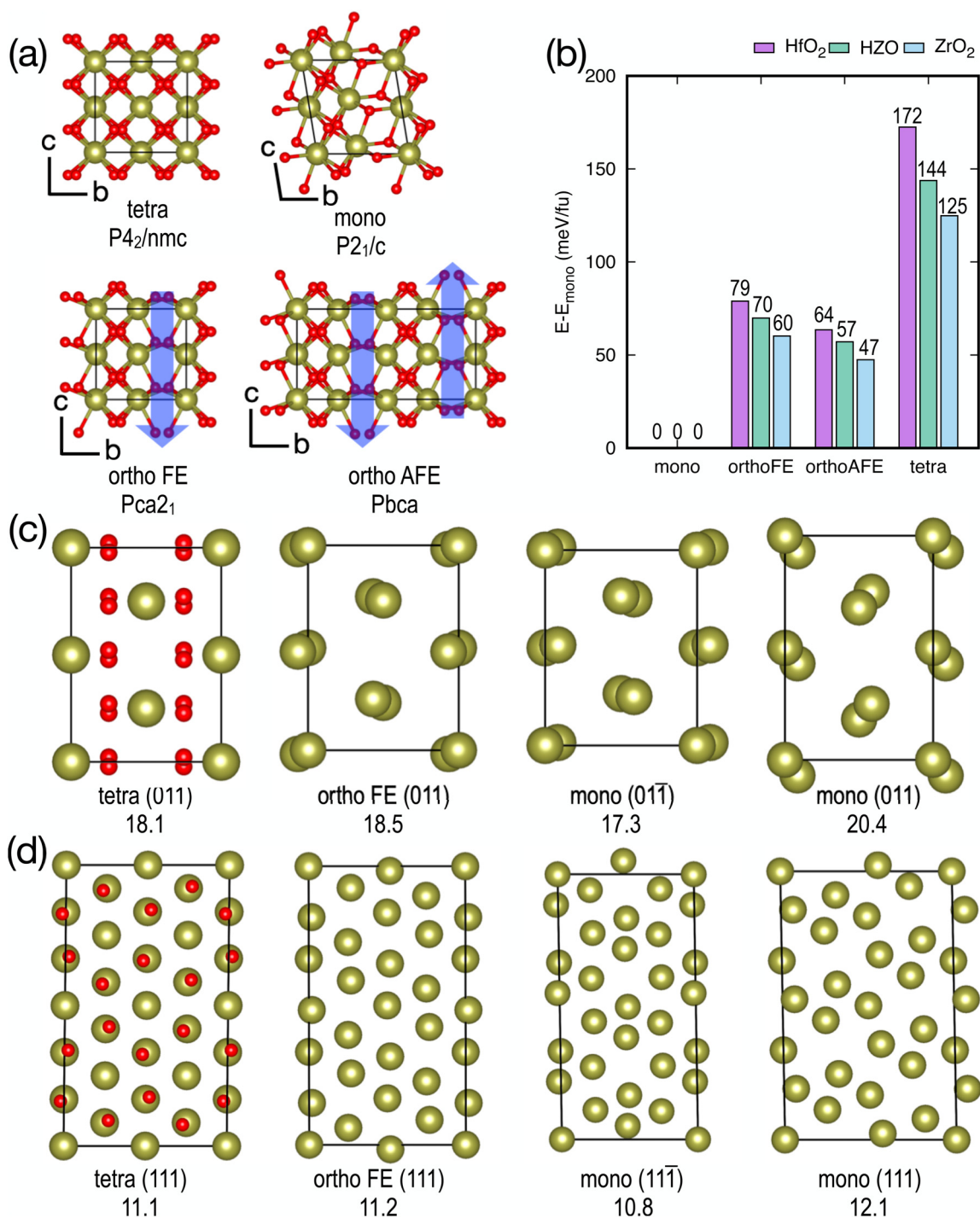
FIG. 1. Atomic structures of HZO polymorphs: (a) unit cells of the polymorphs for antiferroelectric tetragonal $P4_2/nmc$, paraelectric monoclinic $P2_1/c$, ferroelectric ortho-rhombic $Pca2_1$, and antiferroelectric orthorhombic $Pbca$. The blue arrows indicate displaced O atoms. (b) Relative energies of the HfO_2, HZO, and ZrO_2 polymorphs with respect to the ground state of paraelectric monoclinic $P2_1/c$ phase in meV/fu. (c) Rotated supercells for modeling biaxial strain along {011}. (d) Rotated supercells for modeling biaxial strain along {111}. The area per formula unit ($\mathring{A}^2$/fu) is shown on the bottom of each configuration. Note that the monoclinic $P2_1/c$ phase shows two non-equivalent planes for both {011} and {111}. O atoms are omitted for clarity.

calculations are correct but a separate mechanism must be present to explain the experimental results for {111} oriented films.

The tetragonal P4$_2$/nmc phase, assumed to be antiferroelectric (AFE), is often observed in pure ZrO$_2$ films. The tetragonal ZrO$_2$ phase has a formation energy which is 65 meV/fu higher than the orthorhombic phase and 125 meV/fu higher than the ground state monoclinic phase as shown in Fig. 1(b) and in other reports.[14] The observation of tetragonal ZrO$_2$ likely results from interfacial free energy because ZrO$_2$ tends to form nanocrystalline films due to its lower crystallization temperature compared to HfO$_2$.[15] In addition, nanocrystalline HfO$_2$ and ZrO$_2$ domains embedded in a SiO$_2$ dielectric matrix are known to be tetragonal even in thick films (i.e., 200–700 nm), which is again consistent with a favorable interfacial free energy for tetragonal phases with surrounding dielectric phases[16] but such effects have not yet been validated by DFT calculations. Only a few related DFT calculations can be found recently to take into account the HZO interfaces. For instance, Blaise has demonstrated a metal-ferroelectric-metal capacitor model of TiN/ Si-doped HfO$_2$/TiN in DFT calculations, and quantitatively estimated a depolarization field of 2.5 MV/cm,[17] which agrees with experiments.

In this paper, atomistic mechanisms using DFT models are provided for the two key experimental observations described above. First, by carefully examining the crystal structures of various polymorphs in HZO, two distinct planes of the monoclinic phase have been identified, one of which shows higher surface atomic density than the FE phase and is observed experimentally on common electrodes. Crystallization of amorphous HZO on strongly bound electrodes generates tension due to the crystalline phases having a higher density than the amorphous phase. During post-deposition crystallization of amorphous HZO, the resulting tension will favor the formation of FE orthorhombic HZO compared to the high density plane of the monoclinic phase. Second, stack and 3D models show that a polarization perpendicular to the dielectric–ferroelectric interface has a high interfacial free energy consistent with nanocrystalline ZrO$_2$ spontaneous forming the tetragonal phase and HZO commonly requiring electrical cycling, i.e., a wake-up process, for observation of strong ferroelectric behavior.

II. COMPUTATIONAL DETAILS

DFT calculations are performed in the Vienna *ab initio* software package[18,19] to determine the stabilization mechanisms of HZO thin films. The plane-wave basis set of wave functions is expanded up to a kinetic energy cutoff of 400 eV. The projector augmented wave method is used for the core part.[20] The exchange-correlation functional of Perdew–Burke–Ernzerhof is employed.[21] For the Brillouin zone sampling, Kohn–Sham energy eigenvalues are integrated into reciprocal space on even grids generated by a Monkhorst–Pack[22] scheme with a density of 0.25 $2\pi\text{Å}^{-1}$. The electronic structure self-consistent field optimization is iterated until changes in each of the eigenvalues and the total energy are less than 10^{-4} meV. Atomic positions and lattice parameters are optimized by the conjugate gradient method until the Hellmann–Feynman forces acting on each atom became smaller than 1 meV/Å.

To impose in-plane strain along different orientations of HZO such as {001}, {011}, and {111}, unit cell rotation is performed to orient one of the cell axes to be perpendicular to the plane of interest, which is similar to a previous study.[12] Isotropic change of the initial rotated cell area is imposed to generate in-plane strain. To model the plane-stress condition, i.e., $\sigma_{zz} = 0$, the cell parameter along that orientation is set free to relax while the other two cell parameters are fixed at the designated values. The details of the in-plane biaxial strain can be found in the supplementary material.

To model HZO in a $1 \times 1 \times 1$ cell containing four HfO$_2$ formula units, two of the metal sites are occupied by Hf, while the other two sites are occupied by Zr. All the possible configurations of HZO alloys are determined to be energetically degenerated within the sub-meV/fu limit for $1 \times 1 \times 1$ cell, and the difference in energy is less than 2 meV/fu for doubled cells. Therefore, the most energetically stable configuration of the ordered HZO alloy is chosen for all the calculations below.

III. RESULTS AND DISCUSSION

Figure 1(a) shows various polymorphs of HZO. Derived from a cubic parent phase (fluorite), all the polymorphs show similar atomic arrangements; the metal ions (Hf/Zr) form a face-centered cubic (FCC) lattice framework with the O atoms occupying all eight tetrahedral sites of the FCC lattice. Each of the O atoms is displaced from the cubic symmetric positions (i.e., the center of the tetrahedral site), and the polymorphs are identified by the specific arrangements of the displaced O atoms as shown in Fig. 1(a). Note that the Pca2$_1$ phase (ortho FE) represents a non-centrosymmetric ferroelectric phase with spontaneous dipoles as marked by blue arrows in Fig. 1(a). However, the ortho FE phase is a metastable phase in the pure bulk state with its formation energy higher by 60–79 meV/fu (ZrO$_2$ to HfO$_2$) than the ground state P2$_1$/c phase (mono) as seen in Fig. 1(b). The Pbca phase (ortho AFE) shows a similar atomic arrangement as the ortho FE but the displacements of O atoms are switched in every other unit cell of the ortho FE to form a centrosymmetric phase.

Figure 1(b) shows that the tetragonal P4$_2$/nmc phase (tetra AFE) is 65–93 meV/fu (ZrO$_2$ to HfO$_2$) higher in energy than the ortho FE in static DFT calculations (i.e., at 0 K) but it is known that the tetra AFE is the ground state at relatively high temperature,[23] indicating that the difference in entropic contribution from phonons plays a role. Note that at zero fields, the tetra AFE does not have local dipoles in contrast to the ortho AFE as shown in Fig. 1(a), and the tetra AFE phase is known to experimentally exhibit paraelectric behavior for weak external electric fields,[24] which is the middle part of the double hysteresis loop of the AFE. Once the external field becomes large, the tetragonal phase transforms into a phase showing a ferroelectric-like electric response, responsible for a hysteresis curve.[24]

Unlike the orthogonal phases, the mono phase has non-equivalent planes with (hkl) and (hk$\bar{l}$) indices where h, k, and l are integers. The mono (01$\bar{1}$) shows higher surface atom density than the mono (011) as shown in Fig. 1(c), e.g., 0.058 and 0.050 fu/Å^2. Similarly, mono (11$\bar{1}$) and mono (111) show higher and lower surface atom densities, respectively, than both tetra (111) and ortho FE (111) as shown in Fig. 1(d); the surface atom densities for tetra

(111), ortho (111), mono (11$\bar{1}$), and mono (111) are 0.090, 0.089, 0.093, and 0.083 fu/Å^2, respectively. This is in agreement with experimental splitting of the x-ray diffraction peaks (2θ) corresponding to tetra (111) or ortho (111) at ~30° into two separate peaks at ~28° and ~32° after monoclinic formation.[23] The peak at the smaller 2θ is more likely corresponds to the mono (11$\bar{1}$) which shows the higher surface atomic density. Experimentally, it is known that mono (11$\bar{1}$) peak is favored in thinner HZO films on the reactive TiN electrodes,[25] where the interfacial effects are expected to play a significant role. This is consistent with the concept that the reactive electrode tightly bonds oxygen thereby favoring the more dense crystal plane of mono (11$\bar{1}$).

The experimental procedures to obtain ferroelectric HZO thin films elucidate the stabilization mechanism for ferroelectricity. In general, as-deposited HZO grown by the thermal atomic layer deposition (ALD) forms an amorphous film, which is subsequently crystallized during thermal annealing over 400 °C.[1,2,25,26] It is hypothesized that reactive metal electrodes such as TiN and W, also help stabilize the FE films,[10] which result in in-plane tension during the crystallization as the film is densified while maintaining strong bonding at the interfaces. It has been previously shown that FE HZO films sandwiched by TiN electrodes after annealing are under tension.[13] Therefore, identifying the distinct planes with different densities and taking into account the strong bond formation at the interfaces play a crucial role to explain properly the hypothesis that in-plane tension generated during the post-deposition annealing might stabilize the ortho FE phase.

Figure 2 shows the energy of HZO polymorphs with varying compositions (i.e., HfO$_2$, Hf$_{0.5}$Zr$_{0.5}$O$_2$, and ZrO$_2$) with in-plane strain perpendicular to the {111} orientation which is the preferred growth direction when HZO is deposited on TiN or W.[1,2,25,26] Here, only the high density plane of the monoclinic ("mono")

phase, or (11$\bar{1}$), is shown since it should be preferred on reactive electrodes and since it is observed experimentally.[25] The curve for the amorphous phase, generated by melt-quench in *ab initio* molecular dynamics, is shown in all cases, confirming higher energy and surface area than the crystalline phases due to the disordered atomic arrangements. When the amorphous phase is crystallized with the strong bonds formed at the interface, it is hypothesized that the volume reduction due to the crystallization will result in in-plane tension, favoring the ortho AFE over the mono phase first, and then the ortho FE phase with further tension. This is consistent with experimental observations that in-plane tension promotes the ferroelectricity but is in contrast with previous computational results, in which the high density monoclinic plane, i.e., (11$\bar{1}$), was not considered.[11,12] Note that the main difference with previous theoretical results is not a calculational method difference but a difference in the choice of the monoclinic {111} orientation for the model system. A clear distinction between the two monoclinic planes [i.e., (111) and (11$\bar{1}$)] helps understand the stabilization mechanism for different growth techniques. For instance, in a DFT modeling study, Liu and Hanrahan showed that the HfO$_2$ ortho FE phase can be favored over the HfO$_2$ mono phase when the HfO$_2$ film is epitaxially grown on a substrate such as Sn-doped In$_2$O$_3$ (ITO) which is lattice matched to the HZO ortho (111) phase. They did not compare the relative stability between HZO ortho (111) and mono (11$\bar{1}$); presumably, they hypothesized the mono (11$\bar{1}$) would not be grown on the ITO substrate. Conversely, in the current study, the exclusive formation of mono (11$\bar{1}$) at the interfaces was hypothesized because the HZO is typically grown on the reactive electrodes (e.g., TiN and W) by the CMOS-compatible ALD process, in which denser atomic planes would be favored due to strong interfacial bonding to the electrodes during post-deposition annealing. This is in accordance with the experimental data.[25]
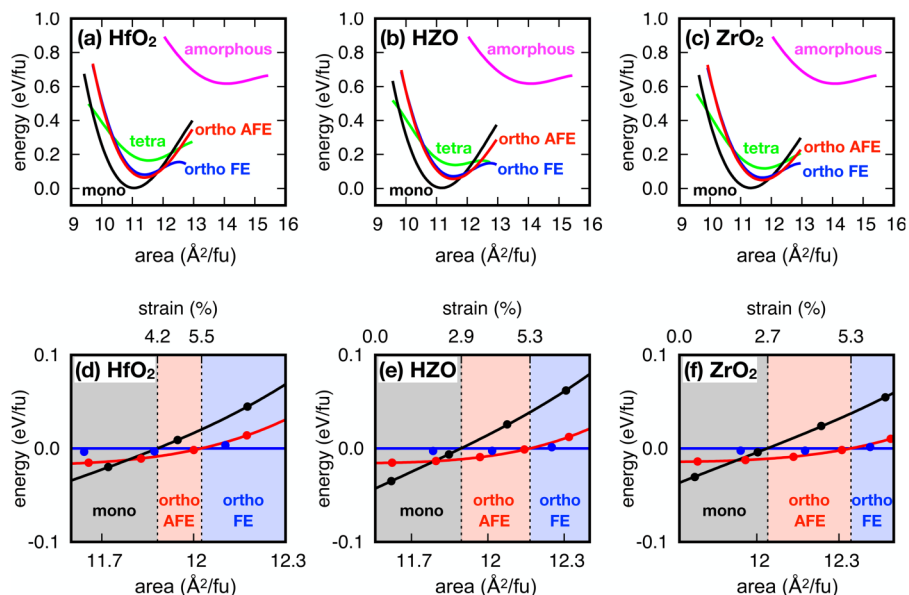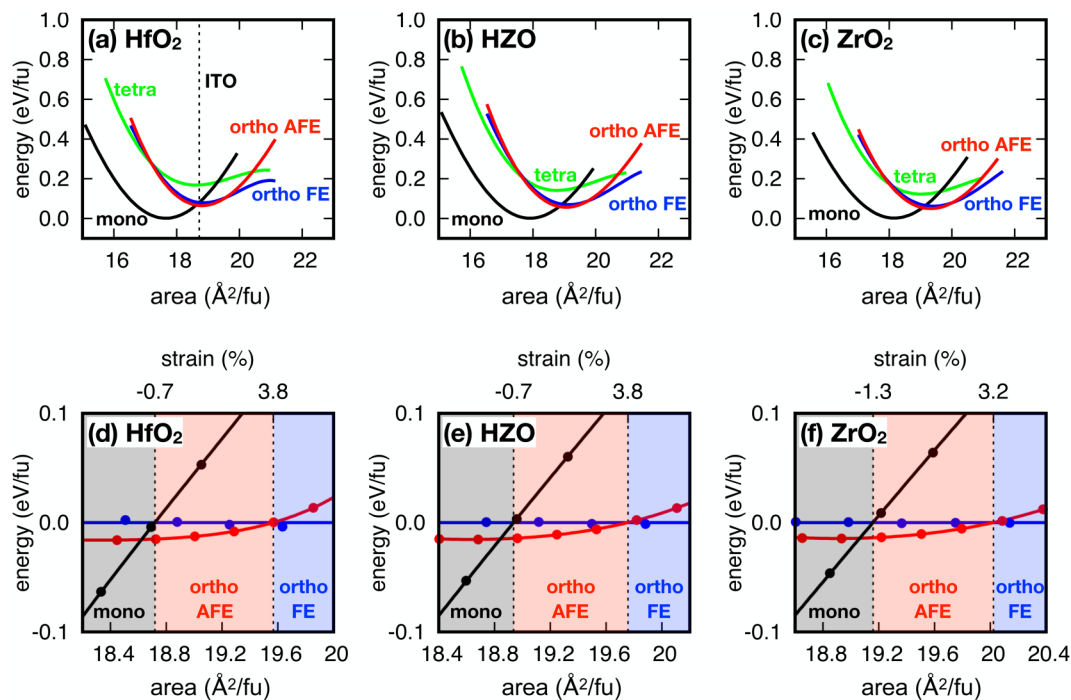

FIG. 2. Energy vs surface area per formula unit along {111}. Energy-area curves for polymorphs of (a) HfO$_2$, (b) HZO, and (c) ZrO$_2$ along {111}. For the monoclinic phase, only the high density plane (11$\bar{1}$) is displayed. Bottom panels show the energies of the polymorphs relative to the ortho FE phase of (d) HfO$_2$, (e) HZO, and (f) ZrO$_2$. The crossover strain values for the ortho FE being more stable than monoclinic and ortho AFE are marked.

The quantitative effect of tension is compared with respect to oxide composition. For pure HfO$_2$, the ortho FE phase becomes more stable than the mono phase when 4.2% in-plane tension is applied with respect to the minimum of the ortho FE phase, while the required tension to stabilize the ortho FE phase are as small as 2.9% and 2.7% for HZO and ZrO$_2$, respectively. The lower amount of in-plane tension being required for the HZO than pure HfO$_2$ to stabilize the ortho FE phase over the mono phase is consistent with experimental results showing that the ferroelectricity is most readily observed in HZO.[6]

While the pure ZrO$_2$ shows the least amount of in-plane tension needed to stabilize the ferroelectricity, it is known that amorphous phase formation is hindered for ZrO$_2$ since it grows in a nanocrystalline phase instead of a purely amorphous phase due to the low crystallization temperature.[15] For HZO, the films are grown in the amorphous phase, and they convert to the ortho FE phase during post-deposition annealing. It has been shown that inserting interfacial HfO$_2$ layers between the electrode and ZrO$_2$, which would direct the growth of ZrO$_2$ into a greater crystal size, enhances the ferroelectricity.[27] As shown in Fig. 1(b), the tetragonal phase is relatively more stable for ZrO$_2$ (65 meV above the minimum of the ortho FE) than either HZO or HfO$_2$ (74 and 93 meV/fu) which is consistent with the experimentally observed easier formation of the tetragonal phase over the orthorhombic FE phase.

In the absence of an external field, the amount of tension needed to stabilize the orthorhombic FE phase over the orthorhombic AFE phase is similar for all the compositions (5.3%–5.5%). However, it has been theoretically shown that an external electric field can further stabilize the orthorhombic FE over the orthorhombic AFE.[11,12] This is consistent with the experimental necessity of external field cycling on the as-annealed films to induce ferroelectricity which is known as the "wake-up" process since ortho AFE will become unstable in the presence of an external field.

Film orientations play crucial roles in the stabilization of the ortho FE phase. Figure 3 shows the energy-area curves for biaxial strain perpendicular to the {011} orientation. Unlike the {111} films which are usually grown on TiN electrodes, the experimental {011} FE films have been grown epitaxially on ITO substrates using pulsed laser deposition (PLD).[28] The bond strains due to epitaxial growth are estimated based on the equilibrium lattice constants of the ITO substrate with a unit area of 18.7 Å^2/fu and the polymorphs of HfO$_2$ as shown in Fig. 1(c). The corresponding epitaxial areal strains for ortho FE (011), monoclinic (011), and monoclinic (01$\bar{1}$) are −1.1%, −7.7%, and 8.8%, respectively, indicating the FE phase is most favorable to grow epitaxially on the ITO substrate. When comparing energies of monoclinic (01$\bar{1}$) and orthorhombic (011) phases, ortho FE can be stabilized without additional mechanical strain because the energy of the ortho FE phase is

FIG. 3. Energy vs surface area per formula unit along {011}. Energy-area curves for the polymorphs of (a) HfO$_2$, (b) HZO, and (c) ZrO$_2$ along {011}. For the monoclinic phase, only the high density plane (01$\bar{1}$) is displayed. Bottom panels show the energies of the polymorphs relative to the ortho FE phase of (d) HfO$_2$, (e) HZO, and (f) ZrO$_2$. The crossover strain values for the ortho FE being more stable than monoclinic and ortho AFE are marked.

lower than that of the monoclinic phase at the minimum of the ortho FE phase in agreement with experiment.[28] In these cases, a thermal annealing step to generate tension during synthesis is not required. Furthermore, the required amount of in-plane tensile strain to stabilize the ortho FE over the ortho AFE ranges 3.2%– 3.8% for {011} which is even smaller than the case of {111} (5.3%– 5.5%). This indicates that the amount of field cycling, or "wake-up," process can be avoided/reduced for the {011} growth in contrast to the {111} case.

In contrast to {111} and {011}, the HZO films along {001} cannot be stabilized either by mechanical strain or epitaxial growth since the energy curve for the monoclinic phase shows a lower energy compared to the orthorhombic ferroelectric phase over a wide range of strains as seen in Fig. S2 in the supplementary material. However, Shimizu et al. have grown an epitaxial film of (001) Y-doped HfO$_2$ on (001) YSZ using PLD and demonstrated that the HfO$_2$ phase progressively changes with substrate Y content from monoclinic to orthorhombic to tetragonal.[29] As the lattice parameters of Y-doped HfO$_2$ and YSZ are sufficiently close to each other, the tetragonal/orthorhombic phases in these films could be stabilized by doping effects or low interfacial free energy due to matching the substrate crystal structures but a full understanding of this system requires further DFT modeling.

To further elucidate the observed FE behavior of HZO and the AFE behavior of nanocrystalline ZrO$_2$ films, stack models with domain boundaries of the tetra and ortho FE phases were constructed for ZrO$_2$ in Figs. 4(a)–4(d) and other compositions in Fig. S3 in the supplementary material. Atomically sharp domain boundaries without a defect within a single grain are built based on the recent experimental report.[30] Stack models with various electric dipole orientations in the ortho FE layers aligned to either x, y, or z are constructed with thicknesses from 3 to 6 unit cells for both the ortho FE and the tetra layers. The tetragonal phase is strained to have the bulk ortho FE cell dimensions and is rotated simultaneously with the ortho FE layer so that the interfacial strain is independent of the dipole orientation. The interface free energy (E_{inter}) is calculated by

$$E_{inter} = (E_{stack} - nE_{tetra} - nE_{ortho})/2A,$$

where E_{stack} is the total energy of the stack. E_{tetra} and E_{ortho} are energies in the bulk state for tetra AFE and ortho FE phases, respectively, with the unit cell volume fixed at ortho FE. The n and A are the tetra/ortho layer thickness and cross-sectional area, respectively. Figure 4(e) shows that the E_{inter} converges with increasing n in all cases. Moreover, the stack with the dipole direction perpendicular to the interface (i.e., along z) shows the highest E_{inter}, which is expected to be due to the electrostatic interactions. This is consistent with the negative capacitance models of Khan et al. showing that perpendicular polarization is destabilized by having a paraelectric in series with ferroelectric HZO.[31] The field due to the spontaneous polarization in the ortho FE region induces the neighboring dielectric layer to be polarized, which will increase the energy of the system. It is observed that unconstrained stack models spontaneously transform into other phases or change polarization directions from perpendicular to parallel to the interface.

Based on a kinetic model proposed previously,[26] the tetra AFE phase forms first during the thermal annealing and is subsequently transformed into the ortho FE phase. Using the internal energy change ($\Delta U = E_{tetra} - E_{ortho}$) and the interfacial free energies (E_S) obtained from the stack models as shown in Fig. 4(e), the energy of ortho–tetra phase transition within a 3D cubic matrix (ΔE) is estimated as a function of the orthorhombic nanocrystal size (m) which is depicted in Fig. 4(f),

$$\Delta E(m) = V(m)\Delta U(m) + \sum_S A_S(m)E_S,$$

where the subscript S in the second term represents the different crystallographic orientations of the {100} interfaces, i.e., (100), ($\bar{1}$00), (010), (0$\bar{1}$0), (001), and (00$\bar{1}$). Here, for simplicity, a symmetric $m \times m \times m$ orthorhombic nanocrystal is assumed to form within the tetragonal matrix although asymmetric precipitates are known experimentally to form within a cubic/tetragonal matrix consistent with the anisotropic E_{inter}.[32] Figure 4(g) shows that the interfacial energy dominates for small-sized crystals, indicated by negative ΔE, while the ΔU term starts to dominate for large crystals when m (the length of the nano crystallites) reaches ~10, which corresponds to a crystal with a length of 5 nm and a volume of 125 nm^3. The results show that for below 5 nm in length, the orthorhombic ferroelectric grains will transform to tetragonal due to high surface free energy, while grains larger than 5 nm will remain in the orthorhombic phase inside the tetragonal matrix due to the higher bulk thermodynamic stability of the orthorhombic phase.

These DFT results can explain the experimental kinetics of crystallization of the film during the cooling process. Starting from the high temperature where each of the grains is tetragonal, if grain growth is suppressed in a rapid cooling process, the DFT calculation predicts the crystallites would remain tetragonal. However, for a slow cooling rate, orthorhombic nanocrystals with sizes greater than the critical size can be formed, and the DFT calculations predict they would convert to the ortho FE phase. The results are shown for HZO but similar results are observed for all three oxides. Note that the effects of point defects are not taken into account in this study but they are known to play an important role[33–35] which is beyond the scope of this study. These results also do not take into account tension which will stabilize both the tetragonal and orthorhombic phases against relaxation to the monoclinic phase. However, the results show that formation of tetragonal films can be favored for ZrO$_2$ if film formation is initiated by nanocrystal formation.

To model the experimentally observed formation of the AFE tetragonal ZrO$_2$ in a paraelectric matrix,[15,16] the interface effects are explicitly taken into account in three-dimensional (3D) DFT models of ferroelectric orthorhombic and tetragonal cores embedded within a cubic matrix as illustrated in Fig. 5(a). The cubic phase is employed as the matrix due to its high symmetry, and it serves as a paraelectric medium. Lattice parameters of the cubic phase are used for both tetragonal and orthorhombic cores to build 3D models with periodic boundary conditions and to model nanocrystals embedded within a matrix. To study the effects of the size of the core on interfacial free energy (Fig. S4 in the supplementary material), the lattice constants of the core and matrix were fixed at
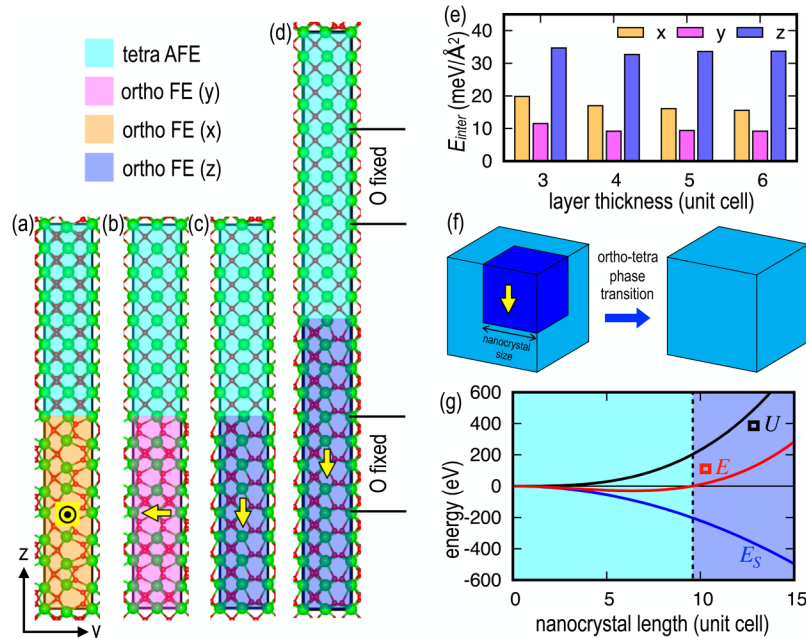
FIG. 4. Transformation of ferroelectric crystallites to tetragonal films. ZrO₂ stack models for tetra–ortho domain boundaries in which each layer is four unit cells thick with polarization orientation along (a) x, (b) y, and (c) z, as marked by yellow arrows. (d) Stack model of polarization along z with a thickness of six unit cells. The O atoms in the two unit cells in the middle of each layer are fixed to prevent phase transition. (e) Interfacial free energy (E_{inter}) of each model with varying polarization direction and layer thickness. (f) Three-dimensional (3D) models of a orthorhombic ferroelectric (blue) nanocrystal embedded within a tetragonal antiferroelectric (light blue) matrix. (g) Thermodynamic model for orthorhombic nanocrystal formation within a 3D tetra matrix as a function of nanocrystal length based on the changes of internal energy (ΔU) and interfacial free energy (E_S). When ΔE is positive, the FE core in the tetragonal matrix is stable. This model takes into account the internal energies from bulk calculations and the interfacial energies in all three directions from (e). The interfacial free energy, E_S, dominates for small-sized crystals, while the ΔU term starts to dominate when m is reached at ∼10, which corresponds to about 5 nm length and 125 nm³ in volume. The results show that the orthorhombic ferroelectric grains below 5 nm in length will transform to tetragonal due to high surface free energy while grains larger than 5 nm will remain in the orthorhombic phase inside the tetragonal matrix. The data shown here are for ZrO₂ but similar DFT results are observed for HfO₂ and HZO.

the equilibrium value for the cores. Note this is in contrast to the lattice constants in Fig. 5 which were fixed at the value for the cubic matrix because when determining the effect of core size on electrostatic interfacial free energy, it is important to ensure that electrostatic effects are dominant regardless of any mechanical strains. Note in real materials, the matrix could be amorphous ZrO₂ or SiO₂ in grain boundaries or amorphous interlayers on the electrode surfaces.[15,16] Unlike the stack models in Fig. 4, in which interface is made along one direction, the dipole in the ferroelectric core in Fig. 5(a) is embedded within the DE matrix and is always pointing to one of the interfaces. Note all the O atoms in the 3D models were fixed at their ideal positions of the corresponding phases to prevent the models in Fig. 5 from converting to a single phase. These 3D models simulate experimental results of nanocrystals embedded within a dielectric matrix such as in Ref. 16. The unfavorable interactions at the FE/DE interface cannot be avoided, and the core of orthorhombic ferroelectric is transformed into the tetragonal phase despite its higher ΔU as seen in Fig. 1(b).

Figure 5(b) shows that the tetragonal cores are significantly lower in energy compared to the orthorhombic cores due to the interfacial free energy. Mechanical strain did not have a significant

influence in this case as shown in Fig. S4 in the supplementary material. The effect of having an AFE tetragonal vs FE orthorhombic core is profound; the AFE tetragonal core is more stable than the FE orthorhombic core by ∼224–252 meV/fu for 3 × 3 × 3 models and by ∼183–189 meV/fu for 2 × 2 × 2 models, despite the bulk AFE tetragonal phase being less stable than the FE orthorhombic phase by 65–93 meV/fu as seen in Fig. 1(b). The overall increase of the energy differences for the 3 × 3 × 3 models compared to the 2 × 2 × 2 models agrees with the prediction in Fig. 4(g) that ΔE becomes more negative with the nanocrystal length up to ∼6 unit cells. The ΔE is the lowest for the pure ZrO₂ partly due to the smaller energy difference compared to HfO₂ and HZO between the orthorhombic and tetragonal phases as in Fig. 1(b), which is consistent with the experiments that tetragonal phase is most prevalent in pure ZrO₂ films,[15,16] together with the low crystallization temperature to form nanocrystals. It has also been shown experimentally that ZrO₂ films with large grain sizes favor the orthorhombic phase,[27] confirming the interfacial effects.

Finally, the role of field cycling, also known as "wake-up," is related to the stability of the antiferroelectric vs ferroelectric phases. Experimentally, the HZO film is grown along {111}; therefore, as
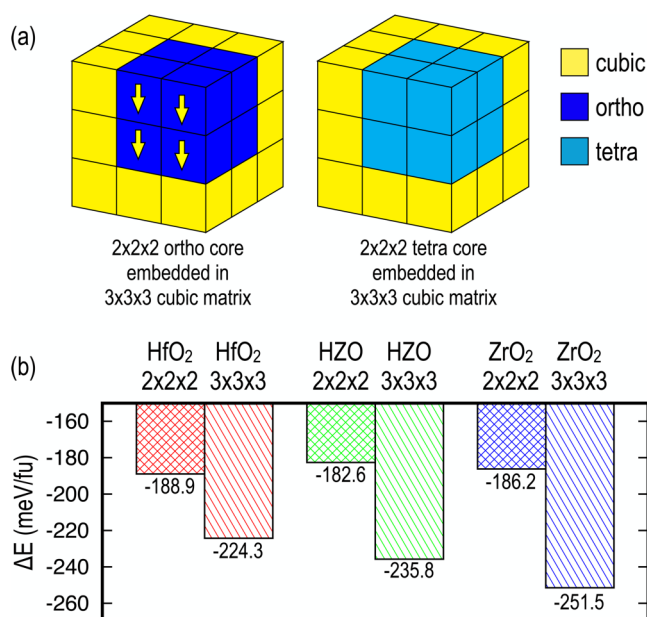
FIG. 5. Three-dimensional core-matrix models. Schematics of the 3D model with 3 × 3 × 3 cubic (yellow) matrix embedding (a) 2 × 2 × 2 orthorhombic ferroelectric cores (blue) and 2 × 2 × 2 tetragonal antiferroelectric cores (light blue), respectively. The cubic phase in the matrix serves as paraelectric layer. Cell sizes for both tetragonal and orthorhombic cores are fixed at values for the cubic matrix. (b) Differences in energy of the 3D models with tetragonal and orthorhombic cores embedded within cubic matrix are calculated with varying core size: energy differences for a 2 × 2 × 2 matrix with ortho FE vs tetragonal AFE 1 × 1 × 1 cores and 3 × 3 × 3 matrix with ortho FE vs tetragonal AFE 2 × 2 × 2 cores. The negative values mean the tetragonal core is more stable than the orthorhombic core due to the presence of the paraelectric matrix. This is in contrast to bulk case where the ortho FE is 65–93 meV/fu more stable than the tetragonal AFE as shown in Fig. 1(b).

described by Blaise et al., there will always be a dipole component pointing to the interface.[17] The results shown in this study indicate that the AFE tetragonal phase or the AFE orthorhombic Pbca phase would be favored due to the unfavorable electrostatic interactions for the FE phase in a dielectric matrix. In addition, grain boundaries are often observed in the films after post-deposition annealing, where paraelectric oxide is likely to form; this could further promote AFE formation over the orthorhombic ferroelectric. However, in the presence of an external field, the ferroelectric phase would be stabilized compared to the non-polar phases as shown in previous DFT calculations.[11,12] This field-aided stabilization of the ferroelectric phase is consistent with the FE HZO film synthesis in general that "wake-up" is necessary to obtain FE behavior.

IV. CONCLUSION

Density functional theory calculations were employed to understand two major phenomena of the phase stabilization for hafnium–zirconium oxide thin films. First, the stabilization of the ferroelectric orthorhombic phase is enabled by in-plane tensile strain if the amorphous film is deposited on top of reactive metal electrodes and is subsequently crystallized by post-deposition annealing. Second, interfacial free energy plays a crucial role to stabilize antiferroelectric tetragonal phase and is consistent with the need for electrical cycling for observation of ferroelectric behavior.

SUPPLEMENTARY MATERIAL

See the supplementary material for the following items: (1) computational details of in-plane biaxial strain, (2) biaxial strain along {001} orientation, (3) interfacial free energies of stack models between tetragonal and orthorhombic phases, and (4) three-dimensional core-matrix models with a varying unit cell volume.

DATA AVAILABILITY

The data that support the findings of this study are available from the corresponding author upon reasonable request.

REFERENCES

[1]T. S. Böscke, J. Müller, D. Bräuhaus, U. Schröder, and U. Böttger, Appl. Phys. Lett. **99**, 102903 (2011).
[2]T. S. Böscke, S. Teichert, D. Bräuhaus, J. Müller, U. Schröder, U. Böttger, and T. Mikolajick, Appl. Phys. Lett. **99**, 112904 (2011).
[3]A. I. Khan, K. Chatterjee, B. Wang, S. Drapcho, L. You, C. Serrao, S. R. Bakaul, R. Ramesh, and S. Salahuddin, Nat. Mater. **14**, 182 (2015).
[4]Z. Fan, J. Chen, and J. Wang, J. Adv. Dielectr. **06**, 1630003 (2016).
[5]T. Schenk, S. Mueller, U. Schroeder, R. Materlik, A. Kersch, M. Popovici, C. Adelmann, S. Van Elshocht, and T. Mikolajick, in *2013 Proceedings of the European Solid-State Device Research Conference (ESSDERC)* (IEEE, Bucharest, 2013), pp. 260–263.
[6]M. H. Park, Y. H. Lee, H. J. Kim, T. Schenk, W. Lee, K. D. Kim, F. P. G. Fengler, T. Mikolajick, U. Schroeder, and C. S. Hwang, Nanoscale **9**, 9973 (2017).
[7]S. L. Weeks, A. Pal, V. K. Narasimhan, K. A. Littau, and T. Chiang, ACS Appl. Mater. Interfaces **9**, 13440 (2017).
[8]H. J. Kim, M. H. Park, Y. J. Kim, Y. H. Lee, W. Jeon, T. Gwon, T. Moon, K. D. Kim, and C. S. Hwang, Appl. Phys. Lett. **105**, 192903 (2014).
[9]G. Karbasian, R. dos Reis, A. K. Yadav, A. J. Tan, C. Hu, and S. Salahuddin, Appl. Phys. Lett. **111**, 022907 (2017).
[10]M. Hyuk Park, H. Joon Kim, Y. Jin Kim, T. Moon, and C. Seong Hwang, Appl. Phys. Lett. **104**, 072901 (2014).
[11]R. Batra, T. D. Huan, J. L. Jones, G. Rossetti, and R. Ramprasad, J. Phys. Chem. C **121**, 4139 (2017).
[12]S. Liu and B. M. Hanrahan, Phys. Rev. Mater. **3**, 054404 (2019).

[13]S. J. Kim, D. Narayan, J.-G. Lee, J. Mohan, J. S. Lee, J. Lee, H. S. Kim, Y.-C. Byun, A. T. Lucero, C. D. Young, S. R. Summerfelt, T. San, L. Colombo, and J. Kim, Appl. Phys. Lett. **111**, 242901 (2017).

[14]S. V. Barabash, J. Comput. Electron. **16**, 1227 (2017).

[15]J. Wang, H. P. Li, and R. Stevens, J. Mater. Sci. **27**, 5397 (1992).

[16]S. V. Ushakov, A. Navrotsky, Y. Yang, S. Stemmer, K. Kukli, M. Ritala, M. A. Leskelä, P. Fejes, A. Demkov, C. Wang, B.-Y. Nguyen, D. Triyoso, and P. Tobin, Phys. Status Solidi B **241**, 2268 (2004).

[17]P. Blaise, MRS Adv. **4**, 2619 (2019).

[18]G. Kresse and J. Furthmüller, Phys. Rev. B **54**, 11169 (1996).

[19]G. Kresse and J. Furthmüller, Comput. Mater. Sci. **6**, 15 (1996).

[20]G. Kresse and D. Joubert, Phys. Rev. B **59**, 1758 (1999).

[21]J. P. Perdew, K. Burke, and M. Ernzerhof, Phys. Rev. Lett. **77**, 3865 (1996).

[22]H. J. Monkhorst and J. D. Pack, Phys. Rev. B **13**, 5188 (1976).

[23]O. Ohtaka, H. Fukui, T. Kunisada, T. Fujisawa, K. Funakoshi, W. Utsumi, T. Irifune, K. Kuroda, and T. Kikegawa, J. Am. Ceram. Soc. **84**, 1369 (2001).

[24]J. Müller, T. S. Böscke, U. Schröder, S. Mueller, D. Bräuhaus, U. Böttger, L. Frey, and T. Mikolajick, Nano Lett. **12**, 4318 (2012).

[25]M. Hyuk Park, H. Joon Kim, Y. Jin Kim, W. Lee, T. Moon, and C. Seong Hwang, Appl. Phys. Lett. **102**, 242905 (2013).

[26]M. H. Park, Y. H. Lee, H. J. Kim, Y. J. Kim, T. Moon, K. D. Kim, S. D. Hyun, T. Mikolajick, U. Schroeder, and C. S. Hwang, Nanoscale **10**, 716 (2018).

[27]S.-H. Yi, B.-T. Lin, T.-Y. Hsu, J. Shieh, and M.-J. Chen, J. Eur. Ceram. Soc. **39**, 4038 (2019).

[28]T. Shimizu, K. Katayama, T. Kiguchi, A. Akama, T. J. Konno, O. Sakata, and H. Funakubo, Sci. Rep. **6**, 32931 (2016).

[29]T. Shimizu, K. Katayama, T. Kiguchi, A. Akama, T. J. Konno, and H. Funakubo, Appl. Phys. Lett. **107**, 032910 (2015).

[30]E. D. Grimley, T. Schenk, T. Mikolajick, U. Schroeder, and J. M. LeBeau, Adv. Mater. Interfaces **5**, 1701258 (2018).

[31]A. I. Khan, "Negative capacitance for ultra-low power computing," Ph.D. thesis (EECS Department, University of California, 2015).

[32]E. H. Kisi, J. Am. Ceram. Soc. **81**, 741 (1998).

[33]L. Xu, T. Nishimura, S. Shibayama, T. Yajima, S. Migita, and A. Toriumi, Appl. Phys. Express **9**, 091501 (2016).

[34]Y. Zhou, Y. K. Zhang, Q. Yang, J. Jiang, P. Fan, M. Liao, and Y. C. Zhou, Comput. Mater. Sci. **167**, 143 (2019).

[35]R. Jiang, Z. Wu, X. Du, Z. Han, and W. Sun, Appl. Phys. Lett. **107**, 013502 (2015).